

Reconstructing People, Places, and Cameras

Lea Müller* Hongsuk Choi* Anthony Zhang Brent Yi Jitendra Malik Angjoo Kanazawa
UC Berkeley

{mueller,hongsuk,anthony_zhang1234,brentyi,malik,kanazawa}@berkeley.edu

* equal contribution

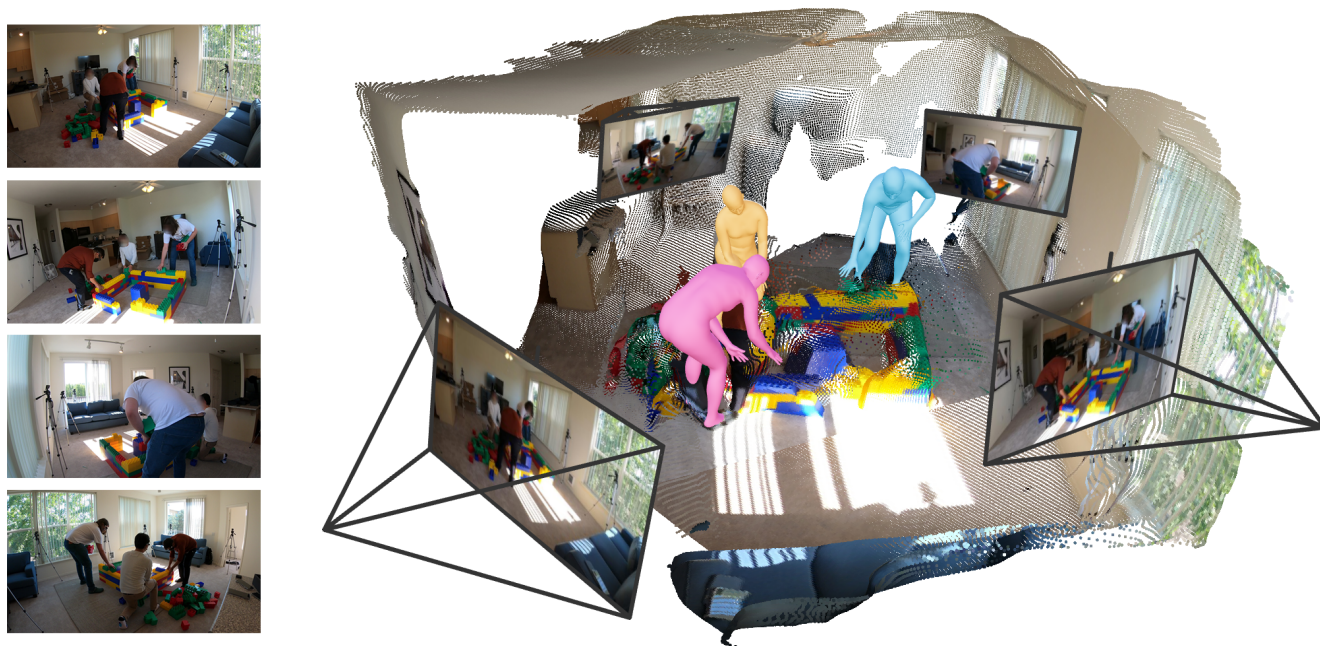


Figure 1. **Humans and Structure from Motion (HSfM)**. We propose a method for the joint reconstruction of humans, scene point clouds, and cameras from an uncalibrated, sparse set of images depicting people. By explicitly incorporating humans into the traditional Structure from Motion (SfM) framework through 2D human keypoint correspondences and leveraging robust initialization from an off-the-shelf model for scene and camera reconstruction, our approach demonstrates that integrating these three elements—people, scenes, and cameras—synergistically improves the reconstruction accuracy of each component. Unlike prior work in SfM and human pose estimation, our method reconstructs metric-scale scene point clouds and camera parameters, informed by human mesh predictions, while situating human meshes in coherent world coordinates consistent with the surrounding environment without any explicit contact constraints.

Abstract

We present “Humans and Structure from Motion” (HSfM), a method for jointly reconstructing multiple human meshes, scene point clouds, and camera parameters in a metric world coordinate system from a sparse set of uncalibrated multi-view images featuring people. Our approach combines data-driven scene reconstruction with the traditional Structure-from-Motion (SfM) framework to achieve more accurate scene reconstruction and camera estimation while simultaneously recovering human meshes. In con-

trast to existing scene reconstruction and SfM methods that lack metric scale information, our method estimates approximate metric scale by leveraging the human statistical model. Furthermore, our method reconstructs multiple human meshes within the same world coordinate system with the scene point cloud, effectively capturing spatial relationships among individuals and their positions in the environment. We initialize the reconstruction of humans, scenes, and cameras using robust foundational models and jointly optimize these elements. This joint optimization synergistically improves the accuracy of each component. We

compare our method with existing methods on two challenging benchmarks, *EgoHumans* and *EgoExo4D*, demonstrating significant improvements in human localization accuracy within the world coordinate frame (reducing error from 3.59m to 1.04m in *EgoHumans* and from 3.01m to 0.50m in *EgoExo4D*). Notably, our results show that incorporating human data into the SfM pipeline improves camera pose estimation (e.g., increasing $RRA@15$ by 20.3% on *EgoHumans*). Additionally, qualitative results show that our approach improves scene reconstruction quality. Our code is available at muelea.github.io/hsfm.

1. Introduction

In recent years, combining deep learning with multi-view geometry has led to significant advances in two key areas: 3D human reconstruction [16, 23] and scene reconstruction [48, 53]. However, progress in these domains has largely evolved independently. Human reconstructions often lack anchoring within their surrounding scenes, while scene reconstructions typically exclude people and fail to recover metric scale. In this paper, we propose a unified framework that bridges these two elements.

We introduce *Humans and Structure from Motion (HSfM)*, a new method that enables the joint reconstruction of multiple human meshes, scene point clouds, and camera parameters within the same metric world coordinate system as shown in Figure 1. From a sparse set of uncalibrated multi-view images featuring people, our approach combines data-driven scene reconstruction with the traditional *Structure-from-Motion (SfM)* framework to enhance the accuracy of scene and camera reconstruction while simultaneously estimating human meshes. The reconstruction process is initialized using robust foundational models for scene reconstruction [53] and human reconstruction [16] and further refined through joint optimization. This optimization incorporates a global alignment loss on scene pointmaps and bundle adjustment based on 2D human keypoint predictions [59], significantly enhancing the accuracy of the three components of world reconstruction—humans, scenes, and cameras. Our overall pipeline is depicted in Figure 2.

Unlike existing approaches to multi-view scene reconstruction [41, 42, 53, 60] and human pose estimation [8, 23, 55], *HSfM* recovers the metric scale of scene point clouds and camera poses while situating human meshes within a unified world coordinate system. The comprehensive output of *HSfM* facilitates the capture and evaluation of spatial relationships among individuals, ensuring consistency with the surrounding environment. Furthermore, unlike prior multi-view human pose estimation methods that depend on precise camera calibration [12, 20, 64], our approach operates with minimal constraints on the capture setup and does

not require prior knowledge of the environment.

Our approach is founded on two key insights. The first insight is that deep learning-based human mesh estimation inherently contains metric scale information, as the predictions reflect the statistical human size present in the training datasets, thereby constraining the scale of the scene. The second insight is that robust 2D human keypoint predictions and 3D human mesh estimations provide precise correspondences and reliable initial 3D structures for bundle adjustment. Note that for the purpose of this work, we assume known re-identification of people across camera views.

We evaluate our approach on two challenging benchmarks, *EgoHumans* [24] and *EgoExo4D* [17], which feature individuals participating in a variety of indoor and outdoor activities across diverse environments. We assess the accuracy of human mesh reconstruction by comparing our method to other approaches that estimate human poses in a world coordinate frame [56]. Additionally, we compare camera pose accuracy against learning-based dense scene reconstruction methods, such as *DUST3R* [53] and *MASt3R* [26]. Our approach demonstrates substantial improvements in camera pose estimation compared to existing methods while accurately positioning individuals within the scene. Specifically, it achieves approximately a 3.5-fold improvement in human metrics, reducing the human world location error from 3.51m to 1.04m on *EgoHumans*, and delivers camera metric improvements of approximately 2.5 times compared to the most relevant baseline [55]. These results underscore the effectiveness of our method, which leverages the joint reconstruction of multiple human meshes, scene point clouds, and cameras, supported by robust initialization for humans [16] and cameras [53]. We further validate our design through ablations which show the synergy between humans, scenes, and cameras. Our qualitative results highlight that the joint optimization of people (multiple humans), places (scenes), and cameras not only enhances human localization but also improves scene reconstruction and camera pose estimation.

In summary, we present *Humans and Structure from Motion (HSfM)*, which provides a comprehensive representation of the world—encompassing people, places, and cameras—marking a step forward in understanding complex real world environments.

2. Related Work

Research in multi-person mesh reconstruction and *Structure from Motion* has seen substantial progress showing remarkable domain-specific results (see Tab. 1). Building on these foundational works, our approach unifies these areas.

Structure from Motion. *Structure from Motion (SfM)* [5, 15, 19] aims to reconstruct camera poses and 3D scene geometry from a set of images by establishing pixel correspondences across views. Traditional SfM Meth-

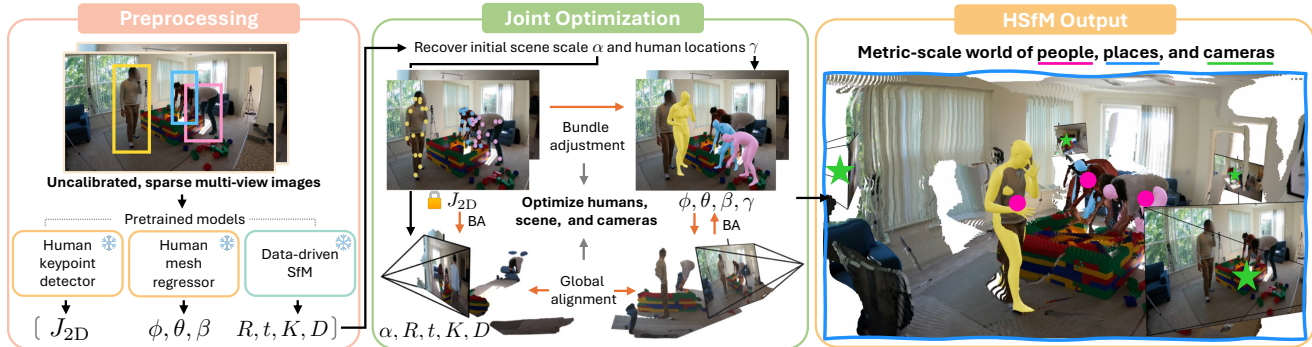


Figure 2. **Pipeline of Humans and Structure from Motion.** Our method processes synchronized images from an uncalibrated multi-view camera setup with known person correspondences across views. We utilize pretrained networks to estimate 2D human keypoints per image [59], 3D human mesh [16], scene point clouds in a *pointmap* representation, and camera intrinsic and extrinsic parameters [53]. We first initialize these estimates in a common world coordinate system by recovering the scene scale α and human locations (global translation in the world coordinate) γ , as described in Section 4.1. We then jointly optimize humans, the scene, and cameras using bundle adjustment based on 2D human keypoints, 3D human meshes, and a global alignment loss that merges per-view pointmaps into the same world space.

	Local Pose	Multi-Person	Stat. Scale	Camera	Places
HMR2 [16, 23]	✓	✗	✗	✗	✗
Multi-HMR [2]	✓	✓	✓	✗	✗
SLAHMR [61]	✓	✓	✓	✗	✗
UnCaliPose [55]	✓	✓	✓	✓	✗
DUST3R [53]	✗	✗	✗	✓	✓
MAS3R [26]	✗	✗	✓	✓	✓
HSfM	✓	✓	✓	✓	✓

Table 1. **Comparison of methods across different features.** Previous works in human pose estimation like HMR2, SLAHMR, Multi-HMR, and UnCaliPose has made great progress in reconstructing body poses in single- and multi-person setups from images. Recent methods like DUST3R and MAS3R are able to recover accurate camera poses and scene points clouds (places). This includes reconstructions with statistically correct scale (Stat. Scale) which can be obtained from human body models, *e.g.* in SLAHMR, or, as in MAS3R, from world knowledge. Our approach, HSfM, is the first to jointly reconstruct multiple people, scene, and cameras from sparse uncalibrated multi-view images.

ods [1, 9, 10], such as COLMAP [41, 42] employs keypoint detection, matching based on locally invariant descriptors [4, 30, 40], and incremental bundle adjustment to estimate camera poses and sparse 3D points. However, these traditional approaches are highly sensitive to noise at each stage of their sequential pipeline and require specific conditions for input, such as a large number of camera views with substantial overlapping image areas.

Learning-based SfM methods replace one or more components of the traditional SfM pipeline with data-driven approaches [3, 11, 28, 39, 62]. Recently, dense matching-based SfM [7, 21, 45, 50, 51, 70] has shifted from sparse keypoints to dense, data-driven approaches. DUST3R [53] and more recent works [13, 26] exemplify this by predicting dense 3D pointmaps without requiring camera calibration.

However, as these methods primarily focus on scene structure, they do not estimate human poses and face challenges in reconstructing pixels corresponding to people. In contrast, our approach robustly recovers both human poses and scene structure simultaneously.

SfM with Humans. Several recent works have leveraged humans in the scene as cues to overcome the limitations of traditional Structure from Motion (SfM) methods in challenging scenarios with minimal overlap or wide baselines. Ma et al. [32, 36] introduce the concept of Virtual Correspondences (VCs), which are pairs of pixels from different images whose camera rays intersect in 3D space, even if the points are not co-visible. Similarly, Xu et al. [58] addressed wide-baseline multi-camera calibration by employing 2D keypoint associations from people across different cameras, obtained by person re-identification methods. Xu and Kitani [56] extended this work by sequentially solving for person re-identification, camera pose estimation, and 3D human pose estimation using multi-view geometry and bundle adjustment in an optimization pipeline. While our approach aligns with this line of research, it differs by jointly optimizing people, places (scene pointmaps), and cameras.

Multi-view human reconstruction. In controlled environments with known camera parameters, multi-view reconstruction leverages geometric consistency for accurate 3D pose estimation, reducing single- and multi-person tasks to a triangulation problem [49] with a long history of research. Recent works explore setups with unknown camera poses by employing end-to-end learning methods that jointly estimate camera parameters and 3D poses [18, 63]. However, these methods are often limited to single-person scenarios [63] or do not incorporate scene context [18]. Existing multi-person methods focus on re-identification [6, 12, 22] or, for video, on re-identification and tracking [20].

In contrast to previous work, our approach does not require camera calibration. Instead, we leverage the human body structure and data-driven SfM methods to achieve accurate human pose and camera estimates.

3. Preliminaries and Notation

Setup. Our method takes as input an uncalibrated, sparse set of C images capturing people in a scene at a single moment in time. We denote each image as I^c , $c = \{1 \dots C\}$, corresponding to each camera, with resolution $H^c \times W^c$. We assume humans have been associated across views. Given this input, our method jointly reconstructs humans, scene, and cameras in a metric 3D world.

Human. For all of the following, we represent humans in the scene via a human body model, SMPL-X [35]. SMPL-X is a differentiable function that maps pose, $\theta \in \text{SO}(3)^J$, and shape, $\beta \in \mathbb{R}^B$ to a triangulated mesh with J joints. This mesh can be placed in the world via two additional parameters, orientation, $\phi \in \text{SO}(3)$, and translation, $\gamma \in \mathbb{R}^3$. We model multiple people, *i.e.* $h \in \{1 \dots H\}$ humans. In summary, a human, h , in the world is defined via

$$H^h = \{\phi^h, \theta^h, \beta^h, \gamma^h\}. \quad (1)$$

Cameras. To project 3D points onto an image, $I \in \mathbb{R}^{H \times W \times 3}$, we use a perspective camera model with intrinsics, $K \in \mathbb{R}^{3 \times 3}$ with focal lengths (f_x, f_y) and principal point $(W/2, H/2)$, and extrinsics with rotation, $R \in \text{SO}(3)$, and translation, $t \in \mathbb{R}^3$. Existing methods produce camera estimates that are not necessarily scaled to real-world size. To address this, we introduce a scaling parameter, α , which adjusts the distance between cameras while preserving their relative directions. With these parameters a 3D point, x^{3D} can be projected to 2D via

$$x_{2D} = K(Rx_{3D} + \alpha t). \quad (2)$$

The pixel coordinates, $(u', v') = (\frac{u}{w}, \frac{v}{w})$ are obtained from $x_{2D} = [u, v, w]^T$. K^c and R^c/t^c denote the in- and extrinsics of camera $c \in \{1, \dots, C\}$.

Scene. We represent the scene via per-view pointmaps [53], $S \in \mathbb{R}^{W \times H \times 3}$, a dense pixel-aligned 3D location for its corresponding image I in the world coordinate frame. S^c denotes the pointmap of an image c . A nice property of pointmap formulations is that we can express them through camera estimates and depth maps. For an image pixel (i, j) , its corresponding pointmap’s world coordinate can be written as

$$S_{i,j} = \alpha(R^T[K^{-1}D_{i,j}[i, j, 1]^T] - R^T t). \quad (3)$$

This formulation unprojects a pixel (i, j) using its depth value $D_{i,j}$ and K , and maps it to the world coordinate system through R^T , $-R^T t$, *i.e.* the *camera-to-world* transform defined by R and t , and scaling.

4. Humans and Structure from Motion

Our method takes as input an uncalibrated, sparse set of images capturing people in a scene at a single moment in time. Given this input, our goal is to jointly estimate each person’s human parameters, the scene, and the camera parameters. Our key insight is that jointly reasoning about people, scene structure, and cameras improves all three aspects of reconstruction. To achieve this, we integrate global scene optimization from recent scene reconstruction methods with the traditional Structure-from-Motion (SfM) formulation. This integration leverages 2D human keypoints as reliable correspondences and 3D human meshes as robust 3D structures for bundle adjustment. Please also refer to Figure 2.

Our joint optimization approach has several advantages. By incorporating human mesh predictions, the method introduces metric scale into the reconstruction process, leveraging statistical information about human body dimensions. The cameras and 2D human keypoints enable precise positioning of individuals within the world coordinate system, allowing for the recovery of their heights and relative distances. Additionally, correspondences of 2D human keypoints enhance camera calibration, which in turn improves scene reconstruction. The scene structure further stabilizes the camera pose registration, creating a feedback loop that refines the overall system. The result is a globally consistent reconstruction of humans, scenes, and cameras, providing a comprehensive understanding of the environment. Since this is an under-determined problem, we take advantage of data-driven 3D human [16] and scene [53] reconstruction methods to provide initializations. Note that our method can easily integrate other mesh regressors tailored towards estimating non-standard body size such as BEV [46].

4.1. Initialization of World

The initial estimates of humans, scene structure, and cameras are derived from different networks and therefore exist in separate coordinate systems. Our objective is to align these components within a unified world coordinate system, a process we refer to as the initialization of the world. To achieve this, we estimate the metric scale that aligns the scene pointmaps and cameras with the humans.

One may simply start the optimization by setting the scale $\alpha = 1$. However, since SfM reconstructions are up-to-scale, the magnitude of t may vary significantly in every reconstruction. If the SfM scene is too small relative to people, cameras may be in-front of the humans, *e.g.* when the scene is placed inside the human mesh, leading to degenerate solutions. Setting alpha to arbitrary big value can prevent this, but makes the problem prone to local minima.

We propose an analytical method to approximate a consistent reconstruction using data-driven outputs of 2D/3D human keypoints and camera parameters. Initially, we roughly position individuals within the scene by estimat-

ing γ , based on the predicted 2D/3D human keypoints and the focal length from \tilde{K} , following a similar approach to Ye et al. [61]. Next, we calculate the initial scale α of the data-driven SfM-predicted world by aligning the data-driven with human-centric camera positions.

Specifically, we first obtain each camera’s rotation, \hat{R}^c , using the estimated 3D human body orientation, $\tilde{\phi}$. This leverages the fact that the human’s orientation should remain consistent in the world coordinate frame across different views. Assuming a reference camera, c_1 , and an anchor person, $\tilde{\phi}^h$, we recover each camera’s rotation by solving

$$(\hat{R}^c)^\top = (R^{c_1})^\top \tilde{\phi}^{hc_1} (\tilde{\phi}^{hc})^\top. \quad (4)$$

We pick the anchor person h based on the best view coverage w.r.t. to the 2D joint confidence scores.

We estimate the camera translation by first estimating the location of the person γ in the world using the data-driven focal length prediction from \tilde{K} and the size of the predicted human following the similar triangle ratio using the average 2D and 3D bone lengths as done in Ye *et al.* [61]. Because the human position in the world coordinate frame should remain consistent when viewed from any camera, we recover camera position T^c in the world coordinate frame via

$$\hat{T}^c = \tilde{\gamma}^{c_1} - (\hat{R}^c)^\top \tilde{\gamma}^c. \quad (5)$$

Finally, given the camera positions \hat{T} derived from the humans and the data-driven camera position predictions \tilde{T} , we solve a least-squares problem to compute $\hat{\alpha}$, which aligns the scene pointmap \mathcal{S} and the camera translation t with the metric-scale world defined by the humans \tilde{H} . The scaling factor $\hat{\alpha}$ provides a reasonable approximation of the metric scale. For the initial estimates of \tilde{H} , we rely on an estimate from a reference camera in practice. Please see the project page supplementary video for an animated illustration.

4.2. Reconstructing People, Places, and Cameras

After initializing the world, we jointly optimize the humans, depth maps, and cameras using a global scene optimization loss and bundle adjustment guided by 2D human keypoint predictions. The objective function is defined as follows:

$$\min_{\{\alpha, \gamma, \beta, \phi, \theta, R, t, K, D\}} L_{\text{Humans}} + \lambda L_{\text{Places}}. \quad (6)$$

To gradually guide the optimization towards the global minimum, we first optimize $\{\alpha, \gamma, \beta\}$ with $\lambda = 0$. Then, we set λ and optimize $\{\gamma, \beta, \phi, \theta, R, t, K, D\}$. The result of this optimization is a metric-scale world with consistent humans, scene, and cameras.

Bundle adjustment based on human keypoints: We define the bundle adjustment objective as follows:

$$L_{\text{Humans}} = \frac{1}{HC} \sum_{c=1}^C \sum_{h=1}^H L_J^{ch} + \frac{1}{H} \sum_{h=1}^H L_\beta^h. \quad (7)$$

The term L_J denotes the re-projection error between the 3D joints of the current estimate with the estimated camera and detected 2D keypoints by ViTPose [59]:

$$L_J^{ch} = \frac{1}{b_{2D}^{ch}} \|c_{2D}^{ch}(J_{2D}^{ch} - K^c(R^c J_{3D}^h + \alpha t^c))\|_2 \quad (8)$$

The keypoint loss for each person, h , and camera, c , is normalized by the bounding box height b_{2D}^{ch} of the 2D human detection and detected keypoints weighted by their estimated confidence scores c_{2D}^{ch} . We further regularize human body shape, $\tilde{\beta}$, to stay close to the average shape of the human body model:

$$L_\beta^h = \|\beta^h\|_2. \quad (9)$$

The output of this optimization is people in plausible size and locations in the world coordinate frame. Please refer to the supplementary material for implementation details.

Global scene optimization: We adapt the global alignment loss from DUST3R [53], which originally optimizes camera and world pointmaps. Intuitively, this loss takes pairs of cameras, say A and B (c_i and c_j), with the predicted content of c_i in B’s view. The alignment loss transforms this “A’s-content-in-B’s-view” to the world coordinate frame where it’s compared against the optimized global scene pointmap, which is A’s content in the world.

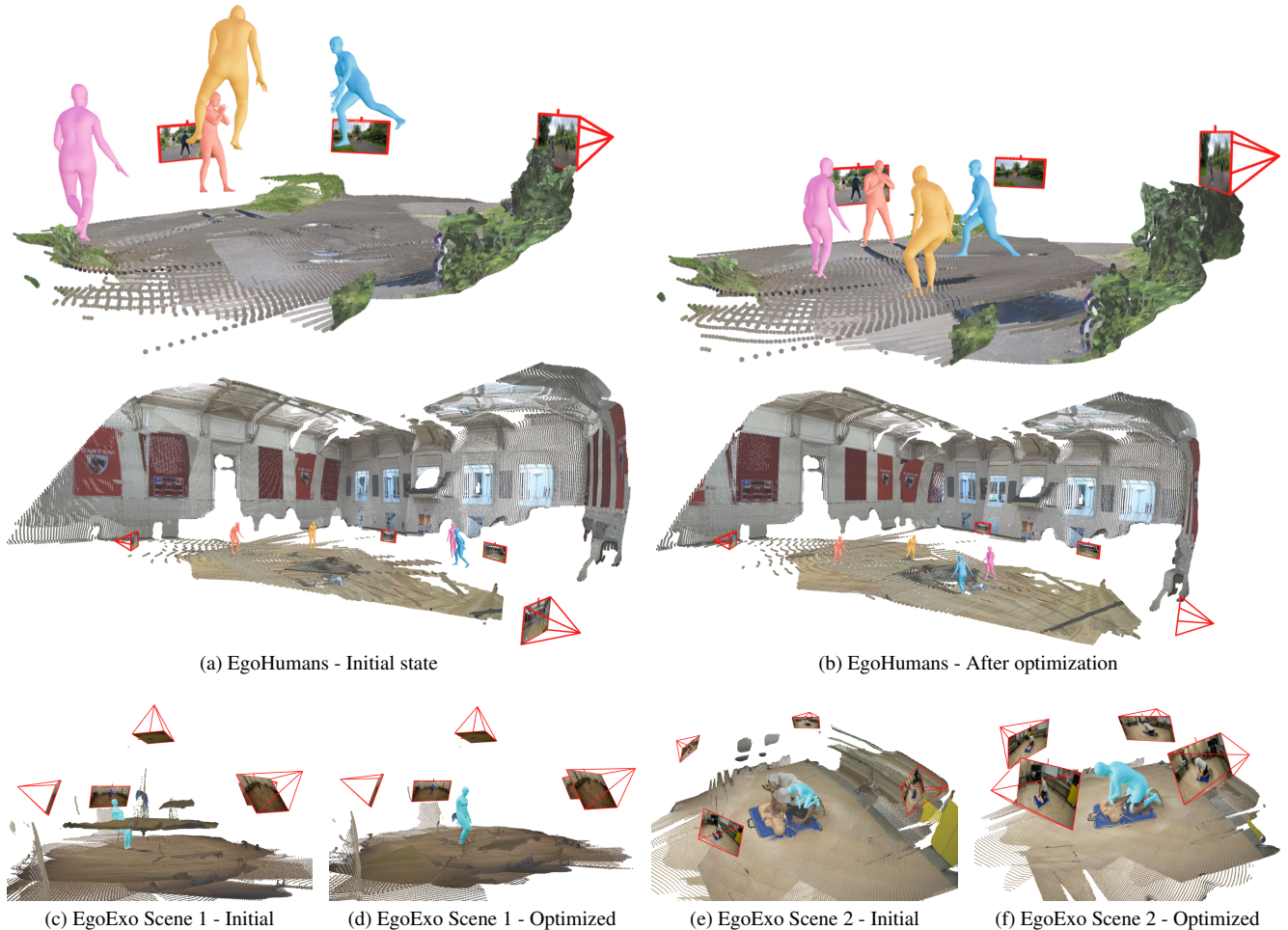
More formally, the global alignment loss aligns per-view pointmaps into a joint world space, *i.e.* $\{\mathcal{S}^c \in \mathbf{R}^{H \times W \times 3}\}$ for $c = 1 \dots C$. To achieve this, the alignment loss takes cross-view pointmaps X^{c_i, c_j} for two cameras $(c_i, c_j) \in \mathcal{E}$, with $i, j = 1 \dots C$ and \mathcal{E} being the set of all pairs of cameras with $i \neq j$. The notation, X^{c_i, c_j} , describes cross-view pointmaps, meaning that the pointmap X^{c_i} of camera c_i is expressed in the coordinate frame of camera c_j . Pairwise transformation matrices $P^{c_i, c_j \rightarrow w} \in \mathbb{R}^{3 \times 4}$, *i.e.* the transformation matrix for camera pair c_i, c_j that brings c_j ’s content to the world coordinate frame. The global alignment loss term is defined as

$$L_{\text{Places}} = \sum_{(c_i, c_j) \in \mathcal{E}} \sum_{i=1}^{HW} Q_i^{c_i, c_j} \|S_i^{c_i} - \sigma^{c_i, c_j \rightarrow w} P^{c_i, c_j \rightarrow w} X_i^{c_i, c_j}\|, \quad (10)$$

where $Q_i^{c_i, c_j}$ are predicted per-pixel confidence maps. $\sigma^{c_i, c_j \rightarrow w}$ is a scaling factor associated to the pair (c_i, c_j) . Note that different from DUST3R [53], we don’t regularize it to avoid a trivial optimum, since the scale is constrained by humans. We omit σ and P in Eq. 6 for clarity, but they are still optimized together following DUST3R.

5. Experiments

We evaluate HSfM’s effectiveness in terms of human pose estimation within the world coordinate system and camera



(a) EgoHumans - Initial state

(b) EgoHumans - After optimization

(c) EgoExo Scene 1 - Initial

(d) EgoExo Scene 1 - Optimized

(e) EgoExo Scene 2 - Initial

(f) EgoExo Scene 2 - Optimized

Figure 3. **Qualitative results from HsFM.** We show our optimized result on sequences from EgoHumans (top) and EgoExo4D (bottom). Note how in the Initial state (left) people are floating in the air (a), how the scene and human scale is not aligned (e), and how noisy the scene appears (c). Our method resolves these problems by grounding people in the scene (b), recovering plausible metric scale (f), and better camera estimates (d). We achieve this without scene contact constraints, which often require assumptions about the environment—such as flat terrain—or about motion, such as the assumption that humans are always in contact with the ground (i.e., no jumping). For more qualitative results, including a demo on images taken in the wild with a minimal capturing setup, please see our supplementary material.

accuracy, and show qualitative results of our joint optimization on humans, scene pointmaps, and cameras.

Evaluation Datasets: We evaluate on EgoHumans [24] and EgoExo4D [17]. EgoHumans is a multi-view, multi-human benchmark for human pose estimation, featuring videos of 2-4 people in real-world activities. EgoExo4D is a large-scale dataset of people performing tasks like dancing, playing music, or bike repair; see Sup. Mat. for details.

Evaluation Metrics: We report metrics for humans and cameras. For people, we use the Mean Per-Joint Position Error (MPJPE). We report **W-MPJPE**, the metric measured in the world coordinate system, and **PA-MPJPE**, its Procrustes-Aligned version, measuring the local pose accuracy. We introduce Group-Aligned MPJPE, (**GA-MPJPE**), which evaluates the relative distance after Sim(3) alignment

between people. All metrics are reported in meters.

For cameras, we report average camera translation error **TE**, *i.e.* the mean euclidean distance in meters between predicted and ground truth camera translations after SE(3) alignment. TE evaluates accuracy in the metric prediction. We also report the Sim(3) aligned version, **s-TE**. **AE** measures the camera Angle Error, *i.e.* the mean Euclidean distance between predicted and ground truth camera rotation. **RRA** [52] evaluates the Relative Rotation Accuracy by comparing the relative rotation between two predicted cameras with the corresponding ground truth. **CCA** [27] assesses the Camera Center Accuracy by directly comparing the predicted and ground truth camera poses. While Lin et al. [27] reported CCA only after optimal Sim(3) alignment, we provide results for two variants: the default

Method	Human Metrics						Camera Metrics						
	W-MPJPE↓	GA-MPJPE↓	PA-MPJPE↓	TE↓	s-TE↓	AE↓	RRA@10↑	RRA@15↑	CCA@10↑	CCA@15↑	s-CCA@10↑	s-CCA@15↑	
EgoHumans	UnCaliPose* [55]	3.51	0.67	0.13	2.63	2.63	60.90	0.28	0.39	-	-	0.33	0.44
	DUST3R [53]	-	-	-	-	1.15	11.00	0.61	0.74	-	-	0.49	0.74
	MASt3R [26]	-	-	-	4.97	0.92	10.42	0.61	0.74	0.06	0.07	0.65	0.86
	HSfM (init.)	4.28	0.51	0.06	2.37	1.15	11.00	0.52	0.79	0.26	0.38	0.49	0.74
	HSfM (Ours)	1.04	0.21	0.05	2.09	0.75	9.35	0.72	0.89	0.32	0.46	0.75	0.91
EgoExo4D	UnCaliPose* [55]	3.59	-	1.19	2.21	0.98	63.98	0.20	0.31	-	-	0.26	0.37
	DUST3R [53]	-	-	-	-	0.34	10.06	0.81	0.88	-	-	0.64	0.84
	MASt3R [26]	-	-	-	1.03	0.36	9.11	0.81	0.90	0.09	0.17	0.70	0.81
	HSfM (init.)	5.80	-	0.08	1.27	0.34	10.06	0.81	0.88	0.05	0.10	0.64	0.84
	HSfM (Ours)	0.50	-	0.07	1.01	0.34	10.39	0.80	0.89	0.05	0.14	0.70	0.84

Table 2. **Evaluation on EgoHumans and EgoExo4D.** HSfM outperforms existing human and scene reconstruction methods, delivering metric-scale reconstructions for humans, the scene, and cameras within the same world coordinate system. Our approach shows major improvement over the initial estimates HSfM (init.), obtained from DUST3R [53] and HMR2 [16] (Section 4.1), particularly when multiple humans are present in the scene, as seen in EgoHumans, compared to a single individual in EgoExo4D. Additionally, HSfM surpasses MASt3R in metric-scale camera metrics, demonstrating the benefit of human size for recovering scene scale. All baselines and our method use four cameras on EgoHumans and up to six cameras on EgoExo4D. Human and camera translation metrics are reported in meters.

Method	Human Metrics						Camera Metrics					
	W-MPJPE↓	GA-MPJPE↓	PA-MPJPE↓	TE↓	s-TE↓	AE↓	RRA@10↑	RRA@15↑	CCA@10↑	CCA@15↑	s-CCA@10↑	s-CCA@15↑
M0: HSfM (init.)	4.28	0.51	0.06	2.37	1.15	11.00	0.52	0.79	0.26	0.38	0.49	0.74
M1: S & C w/o L_{Humans}	3.94	0.57	0.10	2.13	1.1	10.93	0.52	0.79	0.27	0.40	0.48	0.77
M2: w/o L_{Places}	1.29	0.24	0.05	2.82	0.87	13.02	0.50	0.73	0.16	0.24	0.72	0.88
M3: HSfM (Ours)	1.04	0.21	0.05	2.09	0.75	9.35	0.72	0.89	0.32	0.46	0.75	0.91
HSfM (init.)	3.87	0.70	0.06	1.88	1.15	11.34	0.47	0.77	0.23	0.37	0.38	0.69
1 Human	1.69	0.58	0.06	1.91	1.21	10.31	0.52	0.82	0.27	0.44	0.44	0.68
2 Humans	1.66	0.49	0.06	1.84	1.10	9.41	0.62	0.87	0.33	0.45	0.53	0.75
3 Humans	1.41	0.38	0.06	1.69	0.93	8.21	0.74	0.92	0.32	0.46	0.58	0.78
4 Humans	1.28	0.39	0.06	1.52	0.77	8.11	0.74	0.90	0.34	0.53	0.73	0.90

Table 3. **Ablation study.** We demonstrate the advantages of our joint optimization by removing each terms on the EgoHumans dataset. The results indicate that joint optimization is crucial for achieving a coherent reconstruction of cameras and humans. We also perform an ablation study to investigate how the number of humans included affects both camera and human pose estimation in the world coordinates by varying the number of people to include in the optimization using a subset of EgoHumans containing scenes with four people. The results reveal that the effect scales with the number of humans, highlighting the importance of leveraging multiple individuals.

metric computed after SE(3) alignment, and **s-CCA**, computed after Sim(3) alignment. RRA, CCA, and s-CCA are reported for a threshold τ following the previous literature [13, 27, 52, 53]. Note that W-MPJPE, TE, and CCA evaluate absolute Euclidean error, while GA-MPJPE, PA-MPJPE, s-TE, and s-CCA evaluate errors up to scale. For further details, please refer to the supplementary material.

5.1. Results

We compare human and camera estimation baselines on EgoHumans and EgoExo4D (Tab. 2), including UnCaliPose [55], DUST3R [53], and MASt3R [26]. UnCaliPose jointly reconstructs humans and cameras using SfM but does not reconstruct the scene and relies on ground truth bone lengths during testing. For a fair comparison, we assume known re-identification across views, use ViTPose for UnCaliPose and HSfM, and apply DUST3R’s focal length to UnCaliPose. Since no existing approach jointly estimates

people, places, and cameras at metric scale from sparse multi-view images, we also report HSfM (init.), the state after our initialization in Sec. 4.1.

On EgoHumans, HSfM (init.) outperforms UnCaliPose in scale-normalized human metrics, reducing GA-MPJPE by approximately 24% and PA-MPJPE by over 50%. It nearly doubles relative rotation accuracy compared to UnCaliPose with RRA@10 and RRA@15 improvements of 86% and 100%, respectively. These gains show the strength of leveraging HMR2 and DUST3R for initialization.

Our optimization further improves results: W-MPJPE drops from 4.28m in HSfM (init.) to 1.04m in HSfM, demonstrating the effectiveness of our approach in resolving scale ambiguity and accurately positioning humans within the world. The camera metrics also improve substantially, surpassing DUST3R’s initial outputs and outperforming MASt3R, reducing TE from 4.97m to 2.09m and achieving about seven times better CCA@15. These results

highlight the advantages of incorporating humans into the reconstruction process to achieve a consistent metric-scale world, consistent with the findings of Zhao et al. [68].

Similar trends observed in EgoExo4D further validate the effectiveness of our method. HSfM achieves substantially better human metrics compared to UnCaliPose, reducing W-MPJPE from 3.59m to 0.50m and PA-MPJPE from 0.13m to 0.07m. For metric-scale camera metrics, HSfM outperforms HSfM (init.), improving CCA@15 by 33%. The improvements in scale-invariant camera metrics are smaller than on EgoHumans, likely due to heavy indoor occlusions affecting 2D keypoint predictions and the use of only one person in EgoExo4D. Similarly, MAST3R estimates slightly more accurate camera centers (CCA@10/15) on EgoExo4D while HSfM is on-par and slightly better on the scale-invariant version (s-CCA@10/15). This is likely due to a single person being less effective for estimating scene scale; an effect we ablate in Tab. 3 on EgoHumans where we also observe a single person to be less efficient for estimating scene scale compared to more people. In contrast, EgoHumans benefits from multiple individuals, providing more 2D keypoint correspondences and strengthening optimization. Our ablation study confirms this trend.

Ablations: We validate the importance of jointly optimizing humans, scenes, and cameras in Table 3. The first variant, M1, detaches the gradients from the human loss to the scene and camera parameters while still optimizing all parameters. Essentially, the cameras and scene do not adjust to minimize the human losses. This leads to minor W-MPJPE improvement (4.28m to 3.94m) and slightly higher GA-MPJPE (0.51m to 0.57m). Camera metrics nearly stagnate (RRA@15, CCA@15) since human losses do not influence the optimization of camera and scene. The second variant, M2, optimizes cameras and humans solely based on the human loss, excluding the scene loss. Interestingly, this significantly improves W-MPJPE (4.28m to 1.29m) and GA-MPJPE (0.57m to 0.24m), indicating accurate recovery of human world locations and relative distances. However, the camera metrics degrade considerably: CCA@15 by 36.8%, and RRA@15 by 7.6%. Without scene losses, the structure fails to anchor the cameras and overfits to human keypoints. This behavior is similar to the limitations observed in UnCaliPose, which relies solely on human keypoints for SfM. In contrast, our full method (M3) achieves the best metrics, reducing W-MPJPE and GA-MPJPE to 1.04m and 0.21m, respectively, and increasing RRA@15 by 22% and CCA@15 by 21%. This highlights the importance of jointly optimizing humans, scenes, and cameras to achieve a coherent and accurate metric-scale reconstruction.

We conduct an ablation study to investigate the impact of the number of humans on camera estimation and its subsequent effect on human metrics in the world coordinate system. As shown in the table, adding more humans consis-

tently improves camera pose estimation, particularly by reducing camera translation error. This improvement directly contributes to achieving the lowest W-MPJPE, accurately reconstructing human locations in the world.

The results highlight that increasing the number of humans, *i.e.* introducing more correspondences for Structure-from-Motion (SfM), strengthens the bundle adjustment process. This validates our strategy of integrating global scene optimization techniques from recent scene reconstruction methods with the traditional SfM formulation. Our approach effectively leverages 2D human keypoints as reliable correspondences and 3D human meshes as robust structures to enhance bundle adjustment and produce coherent, metric-scale reconstructions.

Please refer to the supplementary material for an ablation study on camera/scene scale initialization and the impact of the number of cameras.

Qualitative Results: See Figs. 1 and 3 for qualitative results on EgoHumans and EgoExo4D and our Sup. Mat. for an *in-the-wild* demo with images we captured using a minimal setup of just two cell phones. Figure 3 shows intermediate optimization steps, where in the beginning, people are floating around in mid air. After joint optimization, their feet are consistent with the environment, without any explicit contact constraints. The structure also improves as pointmaps are more coherent around the ground. Please note that the human point cloud is not used as prior for human reconstruction, *i.e.* noisy point clouds or gaps do not directly affect the human reconstruction accuracy. Despite clear improvements in human localization, we sometimes observe scenes with slightly uneven ground planes indicating that scene reconstruction remains a challenging problem. Nonetheless, our approach improves camera metrics and scene reconstruction qualitatively (see Fig. S.3).

6. Conclusion

In this work, we propose Humans and Structure from Motion, HSfM, which optimizes humans, cameras, and scenes in a joint framework. We build on the success of data-driven learning in two parallel domains – 2D/3D human reconstruction [16, 59] and scene reconstruction [53]. However, neither of these approaches is able to reconstruct humans, scenes, and cameras coherently. Our experiments verify the synergy between these three elements — integrating human reconstruction into the classic SfM task not only properly places people in the world, but also significantly improves camera pose accuracy. Despite promising results, as optimization-based framework our approach can be sensitive to hyper-parameters. In future work, it would be interesting to explore this synergy in a feed-forward framework with integrated re-ID or leverage recent work like MONSt3R [66] to extend our insights to videos.

Acknowledgements

This project is supported in part by DARPA No. HR001123C0021, IARPA DOI/IBC No. 140D0423C0035, NSF:CNS-2235013, ONR MURI N00014-21-1-2801, Bakar Fellows, and Bair Sponsors. The views and conclusions contained herein are those of the authors and do not represent the official policies or endorsements of these institutions. We also thank Chung Min Kim for her critical reviews on this paper and Junyi Zhang for his valuable insights on the method.

References

- [1] Sameer Agarwal, Yasutaka Furukawa, Noah Snavely, Ian Simon, Brian Curless, Steven M Seitz, and Richard Szeliski. Building rome in a day. *ACM Communications*, 2011. 3
- [2] Fabien Baradel, Matthieu Armando, Salma Galaoui, Romain Brégier, Philippe Weinzaepfel, Grégory Rogez, and Thomas Lucas. Multi-hmr: Multi-person whole-body human mesh recovery in a single shot. *arXiv preprint arXiv:2402.14654*, 2024. 3, 7
- [3] Axel Barroso-Laguna, Edgar Riba, Daniel Ponsa, and Krystian Mikolajczyk. Key.net: Keypoint detection by hand-crafted and learned cnn filters. In *International Conference on Computer Vision (ICCV)*, 2019. 3
- [4] Herbert Bay, Tinne Tuytelaars, and Luc Van Gool. Surf: Speeded up robust features. In *European Conference on Computer Vision (ECCV)*, 2006. 3
- [5] Paul Beardsley, Phil Torr, and Andrew Zisserman. 3d model acquisition from extended image sequences. In *European Conference on Computer Vision (ECCV)*, 1996. 2
- [6] Chao Chen, Georgios Pavlakos, Shihao Zou, Tony Tung, and Katerina Fragkiadaki. Multi-person 3d pose estimation in crowded scenes based on multi-view geometry. *arXiv preprint arXiv:2007.10986*, 2020. 3
- [7] Hongkai Chen, Zixin Luo, Lei Zhou, Yurun Tian, Mingmin Zhen, Tian Fang, David McKinnon, Yanghai Tsing, and Long Quan. Aspanformer: Detector-free image matching with adaptive span transformer. In *European Conference on Computer Vision (ECCV)*, 2022. 3
- [8] Hongsuk Choi, Gyeongsik Moon, and Kyoung Mu Lee. Pose2mesh: Graph convolutional network for 3d human pose and mesh recovery from a 2d human pose. In *European Conference on Computer Vision (ECCV)*, 2020. 2
- [9] David Crandall, Andrew Owens, Noah Snavely, and Daniel Huttenlocher. Sfm with mrfs: Discrete-continuous optimization for large-scale structure from motion. *IEEE Transactions on Pattern Analysis and Machine Intelligence (PAMI)*, 2013. 3
- [10] Hainan Cui, Xiang Gao, Shuhan Shen, and Zhanyi Hu. Hsfm: Hybrid structure-from-motion. In *Proceedings of the IEEE Conference on Computer Vision and Pattern Recognition (CVPR)*, 2017. 3
- [11] Daniel DeTone, Tomasz Malisiewicz, and Andrew Rabbinovich. Superpoint: Self-supervised interest point detection and description. In *CVPR Workshops*, 2018. 3
- [12] Junting Dong, Hujun Bao, and Xiaowei Zhou. Fast and robust multi-person 3d pose estimation from multiple views. In *Proceedings of the IEEE/CVF Conference on Computer Vision and Pattern Recognition (CVPR)*, pages 7792–7801, 2019. 2, 3
- [13] Bardenius Duisterhof, Lojze Züst, Philippe Weinzaepfel, Vincent Leroy, Johann Cabon, and Jerome Revaud. Mast3r-sfm: A fully-integrated solution for unconstrained structure-from-motion. *arXiv preprint arXiv*, 2024. 3, 7
- [14] Sai Kumar Dwivedi, Yu Sun, Priyanka Patel, Yao Feng, and Michael J. Black. TokenHMR: Advancing human mesh recovery with a tokenized pose representation. In *IEEE/CVF Conference on Computer Vision and Pattern Recognition (CVPR)*, 2024. 7
- [15] Andrew W Fitzgibbon and Andrew Zisserman. Automatic camera recovery for closed or open image sequences. In *European Conference on Computer Vision (ECCV)*, 1998. 2
- [16] Shubham Goel, Georgios Pavlakos, Jathushan Rajasegaran, Angjoo Kanazawa*, and Jitendra Malik*. Humans in 4D: Reconstructing and tracking humans with transformers. In *International Conference on Computer Vision (ICCV)*, 2023. 2, 3, 4, 7, 8, 1
- [17] Kristen Grauman, Andrew Westbury, Lorenzo Torresani, Kris Kitani, Jitendra Malik, Triantafyllos Afouras, Kumar Ashutosh, Vijay Baiyya, Siddhant Bansal, Bikram Boote, et al. Ego-exo4d: Understanding skilled human activity from first-and third-person perspectives. In *Proceedings of the IEEE/CVF Conference on Computer Vision and Pattern Recognition*, 2024. 2, 6, 1
- [18] Peter Hardy and Hansung Kim. Unsupervised multi-person 3d human pose estimation from 2d poses alone. *arXiv preprint arXiv:2309.14865*, 2023. 3
- [19] Richard Hartley and Andrew Zisserman. *Multiple View Geometry in Computer Vision*. 2004. 2
- [20] Chun-Hao P. Huang, Hongwei Yi, Markus Höschle, Matvey Safroshkin, Tsvetelina Alexifadis, Senya Polikovsky, Daniel Scharstein, and Michael J. Black. Capturing and inferring dense full-body human-scene contact. In *2022 IEEE/CVF Conference on Computer Vision and Pattern Recognition (CVPR 2022)*, pages 13264–13275, 2022. 2, 3
- [21] Wei Jiang, Eduard Trulls, Jan Hosang, Andrea Tagliasacchi, and Kwang Moo Yi. Cotr: Correspondence transformer for matching across images. In *International Conference on Computer Vision (ICCV)*, 2021. 3
- [22] Amir Kadkhodamohammadi and Nicolas Padoy. A generalizable approach for multi-view 3d human pose regression. *arXiv preprint arXiv:1804.10462*, 2018. 3
- [23] Angjoo Kanazawa, Michael J. Black, David W. Jacobs, and Jitendra Malik. End-to-end recovery of human shape and pose. In *Computer Vision and Pattern Recognition (CVPR)*, pages 7122–7131, 2018. 2, 3, 7
- [24] Rawal Khirodkar, Aayush Bansal, Lingni Ma, Richard Newcombe, Minh Vo, and Kris Kitani. Egohumans: An egocentric 3d multi-human benchmark. *arXiv preprint arXiv:2305.16487*, 2023. 2, 6, 1
- [25] Diederik P. Kingma and Jimmy Ba. Adam: A method for stochastic optimization. In *International Conference on Learning Representations (ICLR)*, 2015. 7

- [26] Vincent Leroy, Yohann Cabon, and Jerome Revaud. Grounding image matching in 3d with mast3r. In *European Conference on Computer Vision (ECCV)*, 2024. 2, 3, 7
- [27] Amy Lin, Jason Y Zhang, Deva Ramanan, and Shubham Tulsiani. Relpose++: Recovering 6d poses from sparse-view observations. *arXiv preprint arXiv:2305.04926*, 2023. 6, 7, 4
- [28] Philipp Lindenberger, Paul-Edouard Sarlin, and Marc Pollefeys. Lightglue: Local feature matching at light speed. In *International Conference on Computer Vision (ICCV)*, 2023. 3
- [29] Miao Liu, Dexin Yang, Yan Zhang, Zhaopeng Cui, James M Rehg, and Siyu Tang. 4d human body capture from egocentric video via 3d scene grounding. In *3DV*, 2021. 7
- [30] David G. Lowe. Distinctive image features from scale-invariant keypoints. *International Journal of Computer Vision (IJCV)*, 2004. 3
- [31] Hao Luo, Youzhi Gu, Xingyu Liao, Shenqi Lai, and Wei Jiang. Bag of tricks and a strong baseline for deep person re-identification. In *Proceedings of the IEEE/CVF Conference on Computer Vision and Pattern Recognition Workshops*, 2019. 1
- [32] Wei-Chiu Ma, Alexander J. Yang, Shenlong Wang, Raquel Urtasun, and Antonio Torralba. Virtual correspondence: Humans as a cue for extreme-view geometry. In *Proceedings of the IEEE/CVF Conference on Computer Vision and Pattern Recognition (CVPR)*, 2022. 3
- [33] Lea Müller, Vickie Ye, Georgios Pavlakos, Michael J. Black, and Angjoo Kanazawa. Generative proxemics: A prior for 3D social interaction from images. 2024. 7
- [34] Maxime Oquab, Timothée Darcet, Théo Moutakanni, Huy Vo, Marc Szafraniec, Vasil Khalidov, Pierre Fernandez, Daniel Haziza, Francisco Massa, Alaaeldin El-Nouby, et al. Dinov2: Learning robust visual features without supervision. *arXiv preprint arXiv:2304.07193*, 2023. 1
- [35] Georgios Pavlakos, Vasileios Choutas, Nima Ghorbani, Timo Bolkart, Ahmed A. A. Osman, Dimitrios Tzionas, and Michael J. Black. Expressive body capture: 3D hands, face, and body from a single image. In *Computer Vision and Pattern Recognition (CVPR)*, pages 10975–10985, 2019. 4, 7
- [36] Georgios Pavlakos, Jitendra Malik, and Angjoo Kanazawa. Human mesh recovery from multiple shots. In *Proceedings of the IEEE/CVF Conference on Computer Vision and Pattern Recognition*, pages 1485–1495, 2022. 3
- [37] Jathushan Rajasegaran, Georgios Pavlakos, Angjoo Kanazawa, and Jitendra Malik. Tracking people by predicting 3d appearance, location and pose. In *Proceedings of the IEEE/CVF Conference on Computer Vision and Pattern Recognition*, 2022. 1
- [38] Nikhila Ravi, Valentin Gabeur, Yuan-Ting Hu, Ronghang Hu, Chaitanya Ryali, Tengyu Ma, Haitham Khedr, Roman Rädle, Chloe Rolland, Laura Gustafson, Eric Mintun, Junting Pan, Kalyan Vasudev Alwala, Nicolas Carion, Chao-Yuan Wu, Ross Girshick, Piotr Dollár, and Christoph Feichtenhofer. Sam 2: Segment anything in images and videos. *arXiv preprint arXiv:2408.00714*, 2024. 2
- [39] Jérôme Revaud, César Roberto de Souza, Martin Humenberger, and Philippe Weinzaepfel. R2d2: Reliable and repeatable detector and descriptor. In *Advances in Neural Information Processing Systems (NeurIPS)*, 2019. 3
- [40] Ethan Rublee, Vincent Rabaud, Kurt Konolige, and Gary R. Bradski. Orb: An efficient alternative to sift or surf. In *International Conference on Computer Vision (ICCV)*, 2011. 3
- [41] Johannes Lutz Schönberger and Jan-Michael Frahm. Structure-from-motion revisited. In *Conference on Computer Vision and Pattern Recognition (CVPR)*, 2016. 2, 3
- [42] Johannes Lutz Schönberger, Enliang Zheng, Marc Pollefeys, and Jan-Michael Frahm. Pixelwise view selection for unstructured multi-view stereo. In *European Conference on Computer Vision (ECCV)*, 2016. 2, 3
- [43] Zehong Shen, Huaijin Pi, Yan Xia, Zhi Cen, Sida Peng, Zechen Hu, Hujun Bao, Ruizhen Hu, and Xiaowei Zhou. World-grounded human motion recovery via gravity-view coordinates. In *SIGGRAPH Asia 2024 Conference Papers*, pages 1–11, 2024. 7
- [44] Soyong Shin, Juyong Kim, Eni Halilaj, and Michael J. Black. WHAM: Reconstructing world-grounded humans with accurate 3D motion. In *IEEE/CVF Conf. on Computer Vision and Pattern Recognition (CVPR)*, 2024. 1, 7
- [45] Jiaming Sun, Zehong Shen, Yuang Wang, Hujun Bao, and Xiaowei Zhou. Loftr: Detector-free local feature matching with transformers. In *Conference on Computer Vision and Pattern Recognition (CVPR)*, 2021. 3
- [46] Yu Sun, Wu Liu, Qian Bao, Yili Fu, Tao Mei, and Michael J Black. Putting people in their place: Monocular regression of 3d people in depth. In *Computer Vision and Pattern Recognition (CVPR)*, pages 13243–13252, 2022. 4, 7
- [47] Yu Sun, Qian Bao, Wu Liu, Tao Mei, and Michael J. Black. TRACE: 5D Temporal Regression of Avatars with Dynamic Cameras in 3D Environments. In *IEEE/CVF Conf. on Computer Vision and Pattern Recognition (CVPR)*, 2023. 7
- [48] Carlo Tomasi and Takeo Kanade. Shape and motion from image streams under orthography: a factorization method. *International journal of computer vision*, 9:137–154, 1992. 2
- [49] Bill Triggs, Paul F. McLauchlan, Richard I. Hartley, and Andrew W. Fitzgibbon. Bundle adjustment—a modern synthesis. In *Vision Algorithms: Theory and Practice*, pages 298–372. Springer, Berlin, Heidelberg, 2000. 3
- [50] Prune Truong, Martin Danelljan, and Radu Timofte. Glunet: Global-local universal network for dense flow and correspondences. In *Conference on Computer Vision and Pattern Recognition (CVPR)*, 2020. 3
- [51] Prune Truong, Martin Danelljan, Luc Van Gool, and Radu Timofte. Learning accurate dense correspondences and when to trust them. In *Conference on Computer Vision and Pattern Recognition (CVPR)*, 2021. 3
- [52] Jianyuan Wang, Christian Ruppert, and David Novotny. Posediffusion: Solving pose estimation via diffusion-aided bundle adjustment. In *International Conference on Computer Vision (ICCV)*, pages 9773–9783, 2023. 6, 7, 4

- [53] Shuzhe Wang, Vincent Leroy, Yohann Cabon, Boris Chidlovskii, and Jerome Revaud. Dust3r: Geometric 3d vision made easy. In *Proceedings of the IEEE/CVF Conference on Computer Vision and Pattern Recognition (CVPR)*, pages 20697–20709, 2024. [2](#), [3](#), [4](#), [5](#), [7](#), [8](#), [1](#)
- [54] Yufu Wang, Ziyun Wang, Lingjie Liu, and Kostas Daniilidis. Tram: Global trajectory and motion of 3d humans from in-the-wild videos. *arXiv preprint arXiv:2403.17346*, 2024. [7](#)
- [55] Yan Xu and Kris Kitani. Multi-view multi-person 3d pose estimation with uncalibrated camera networks. In *British Machine Vision Conference (BMVC)*, 2022. [2](#), [3](#), [7](#)
- [56] Yan Xu and Kris Kitani. Multi-view multi-person 3d pose estimation with uncalibrated camera networks. In *British Machine Vision Conference (BMVC)*, 2022. [2](#), [3](#)
- [57] Yuanlu Xu, Song-Chun Zhu, and Tony Tung. DenseRaC: Joint 3D pose and shape estimation by dense render-and-compare. In *International Conference on Computer Vision (ICCV)*, 2019. [1](#)
- [58] Yan Xu, Yu-Jhe Li, Xinshuo Weng, and Kris Kitani. Wide-baseline multi-camera calibration using person re-identification. In *Conference on Computer Vision and Pattern Recognition (CVPR)*, 2021. [3](#)
- [59] Yufei Xu, Jing Zhang, Qiming Zhang, and Dacheng Tao. Vit-pose: Simple vision transformer baselines for human pose estimation. *Advances in Neural Information Processing Systems*, 35:38571–38584, 2022. [2](#), [3](#), [5](#), [8](#), [1](#)
- [60] Yao Yao, Zixin Luo, Shiwei Li, Tian Fang, and Long Quan. Mvsnet: Depth inference for unstructured multi-view stereo. In *Proceedings of the European conference on computer vision (ECCV)*, 2018. [2](#)
- [61] Vickie Ye, Georgios Pavlakos, Jitendra Malik, and Angjoo Kanazawa. Decoupling human and camera motion from videos in the wild. In *Computer Vision and Pattern Recognition (CVPR)*, 2023. [3](#), [5](#), [1](#), [2](#), [7](#)
- [62] Kwang Moo Yi, Eduard Trulls, Vincent Lepetit, and Pascal Fua. Lift: Learned invariant feature transform. In *European Conference on Computer Vision (ECCV)*, 2016. [3](#)
- [63] Tao Yu, Zerong Zheng, Kaiwen Guo, and Yebin Liu. Multi-view human body reconstruction from uncalibrated cameras. In *Advances in Neural Information Processing Systems (NeurIPS)*, 2022. [3](#)
- [64] Yuming Yuan, Chun-Hao P. Huang, Donglai Xiang, Yufeng Zhou, Mengcheng Xu, Jingwei Huang, Chenxi Jiang, Tzu-Mao Xu, Deva Ramanan, and Michael J. Black. Human: Multi-modal 4d human dataset for versatile sensing and modeling. In *Proceedings of the IEEE/CVF Conference on Computer Vision and Pattern Recognition (CVPR)*, 2022. [2](#)
- [65] Ye Yuan, Umar Iqbal, Pavlo Molchanov, Kris Kitani, and Jan Kautz. Glamr: Global occlusion-aware human mesh recovery with dynamic cameras. In *Proceedings of the IEEE/CVF conference on computer vision and pattern recognition*, pages 11038–11049, 2022. [7](#)
- [66] Junyi Zhang, Charles Herrmann, Junhwa Hur, Varun Jampani, Trevor Darrell, Forrester Cole, Deqing Sun, and Ming-Hsuan Yang. Monst3r: A simple approach for estimating geometry in the presence of motion. *ICLR*, 2025. [8](#)
- [67] Siwei Zhang, Qianli Ma, Yan Zhang, Zhiyin Qian, Taeyun Kwon, Marc Pollefeys, Federica Bogo, and Siyu Tang. Ego-body: Human body shape and motion of interacting people from head-mounted devices. In *European Conference on Computer Vision (ECCV)*, pages 180–200, 2022. [7](#)
- [68] Yizhou Zhao, Hengwei Bian, Kaihua Chen, Pengliang Ji, Liao Qu, Shao-yu Lin, Weichen Yu, Haoran Li, Hao Chen, Jun Shen, et al. Metric from human: Zero-shot monocular metric depth estimation via test-time adaptation. In *The Thirty-eighth Annual Conference on Neural Information Processing Systems*, 2024. [8](#)
- [69] Yizhou Zhao, Tuanfeng Y. Wang, Bhiksha Raj, Min Xu, Jimei Yang, and Chun-Hao P. Huang. Synergistic global-space camera and human reconstruction from videos. 2024. [1](#), [7](#)
- [70] Shengjie Zhu and Xiaoming Liu. Pmatch: Paired masked image modeling for dense geometric matching. In *Conference on Computer Vision and Pattern Recognition (CVPR)*, 2023. [3](#)
- [71] Yuliang Zou, Jimei Yang, Duygu Ceylan, Jianming Zhang, Federico Perazzi, and Jia-Bin Huang. Reducing footskate in human motion reconstruction with ground contact constraints. In *Proceedings of the IEEE/CVF Winter Conference on Applications of Computer Vision*, 2020. [2](#)

Reconstructing People, Places, and Cameras

Supplementary Material

This is the supplementary material for our main paper “Reconstructing People, Places, and Cameras”. We provide additional qualitative results (Sec. S.1), including in-the-wild examples, a discussion of our approach’s limitations (Sec. S.2), ablation studies on the scale initialization and input views (Sec. S.3), evaluation details (Sec. S.4), implementation detail (Sec. S.5), and additional related work (Sec. S.6).

S.1. Additional Qualitative Results

In-the-wild demo. We first present HSfM’s reconstruction results on images captured by two cell phones in Figures S.1 and S.2. The data was captured using a minimal setup consisting of two cell phones, two tripods, and the Riverside app¹ for straightforward time synchronization. Despite this simple setup, our multi-view optimization algorithm successfully handles challenging scenes, such as individuals jumping, without relying on any heuristic contact priors and small data-driven motion priors that previous works [44, 61, 69] use.

Benchmark evaluation. We provide additional qualitative results on EgoExo4D [17] in Figure S.4, showing challenging scenes such as kitchens, humans interacting with objects (e.g., playing the piano), and sports activities like soccer. In Figure S.7, we display further results on EgoHumans [24], demonstrating HSfM reconstructions of multiple people interacting, such as fencing. Figure S.3 show a scene from EgoHumans before and after HSfM optimization.

S.2. Discussion

Our goal is to study the mutual benefits of jointly reconstructing humans, scenes, and cameras. To this end, we assume that the re-identification of people across camera views is known, because misidentified individuals can introduce spurious effects, disrupting the optimization process. Please note that this limitation also applies to UnCaliPose [57]. To ensure a fair comparison and maintain focus on the core objectives of this study, we rely on ground-truth identities in both our approach and UnCaliPose in the main text.

Since re-identification may not be available at test time and manual identification is cumbersome, we tested the feasibility of automating the re-identification process using the re-identification module of UnCaliPose on the EgoHumans dataset [24]. For re-identification, UnCaliPose solves a constrained clustering optimization problem, as-

suming a known number of people in the scene and utilizing re-identification features extracted by an off-the-shelf re-identification network [31]. The re-identification process achieves an accuracy of 51.22% on EgoHumans. The main failure mode occurs with individuals wearing uniforms (e.g., tennis sequences: 12.04% accuracy, volleyball sequences: 25.71% accuracy), where appearance features are difficult to distinguish.

These findings indicate that manual re-identification remains necessary for accurate multi-view reconstruction of the world, including humans. Fortunately, modern tools like LabelMe² simplify this process. Looking ahead, we anticipate that ongoing advancements in large-scale data-model paradigms will significantly improve performance in multi-view re-identification. These advancements may include robust appearance feature matching [34] and the use of geometric similarities, such as human pose and location [16, 37].

While our method achieves good quantitative results, we observe a few failure cases stemming from preprocessing errors in reconstruction and detections. The most common issues arise from erroneous initial camera estimates generated by the scene reconstruction-based SfM[53], particularly in scenes with limited structure, insufficient overlap between images, or large areas affected by radial distortion. In instances where DUST3R[53] fails to detect any cameras, we rely on human-centric camera poses to initialize the optimization. Another source of error involves missing or highly inaccurate keypoint detections, which can occur under conditions of heavy occlusion or poor lighting. In such cases, our method estimates frame-specific cameras solely based on pixel data, without incorporating human constraints. Despite these occasional errors, we find DUST3R, ViTPose [59], and HMR2.0 [16] to exhibit remarkable robustness across a wide range of challenging scenarios.

S.3. Additional Ablation Studies

We analyze the effect of different scale initializations to validate the superiority of the human-centric scaling introduced in Section 4.1 in Table S.1. Without scale initialization ($\alpha = 1.0$), where we directly use the raw DUST3R [53] scene and camera pose outputs as input to our optimization, the W-MPJPE is 11.89m, whereas ours is 1.04m. Additionally, the high metric-scale camera translation errors, such as 6.42m TE, and extremely low RRA values, demonstrate the necessity of proper initialization. This error occurs be-

¹<https://riverside.fm/>

²<https://github.com/wkentaro/labelme>

	Human Metrics						Camera Metrics					
	W-MPJPE↓	GA-MPJPE↓	PA-MPJPE↓	TE↓	s-TE↓	AE↓	RRA@10↑	RRA@15↑	CCA@10↑	CCA@15↑	s-CCA@10↑	s-CCA@15↑
S1: $\alpha = 1.0$	11.89	0.85	0.09	6.42	5.50	121.88	0.01	0.01	0.01	0.02	0.01	0.05
S2: $\alpha = 100.0$	1.94	0.22	0.06	2.17	1.11	15.00	0.68	0.82	0.31	0.45	0.68	0.83
S3: HSfM (Ours)	1.04	0.21	0.05	2.09	0.75	9.35	0.72	0.89	0.32	0.46	0.75	0.91
2 Cam. HSfM (init)	3.73	0.42	0.06	1.53	-	9.81	0.41	0.87	0.08	0.12	-	-
2 Cam. HSfM (Ours)	2.63	0.26	0.05	0.39	-	10.37	0.41	0.91	0.48	0.68	-	-
4 Cam. HSfM (init)	4.26	0.51	0.06	2.36	1.14	10.96	0.52	0.79	0.26	0.38	0.49	0.74
4 Cam. HSfM (Ours)	1.15	0.27	0.06	2.00	0.71	8.92	0.68	0.88	0.35	0.50	0.78	0.93
8 Cam. HSfM (init)	5.06	0.53	0.06	2.36	0.96	7.61	0.71	0.87	0.25	0.40	0.65	0.88
8 Cam. HSfM (Ours)	1.00	0.19	0.05	1.97	0.90	7.41	0.76	0.90	0.41	0.54	0.72	0.88

Table S.1. **Ablation on the number of input view cameras.** We evaluate the performance of HSfM by varying the number of input view cameras and assessing human reconstruction and camera pose estimation in the world coordinate frame. The experiments are conducted on EgoHumans, excluding samples without ground truth camera poses for all views in the specified combinations (2, 4, and 8). Compared to the initialization, our joint optimization improves all human pose and camera pose metrics, regardless of the number of input cameras. We do not report the scaled version of camera translation errors for the 2-camera cases, as the predictions become identical to the ground truth camera translations after scale alignment.

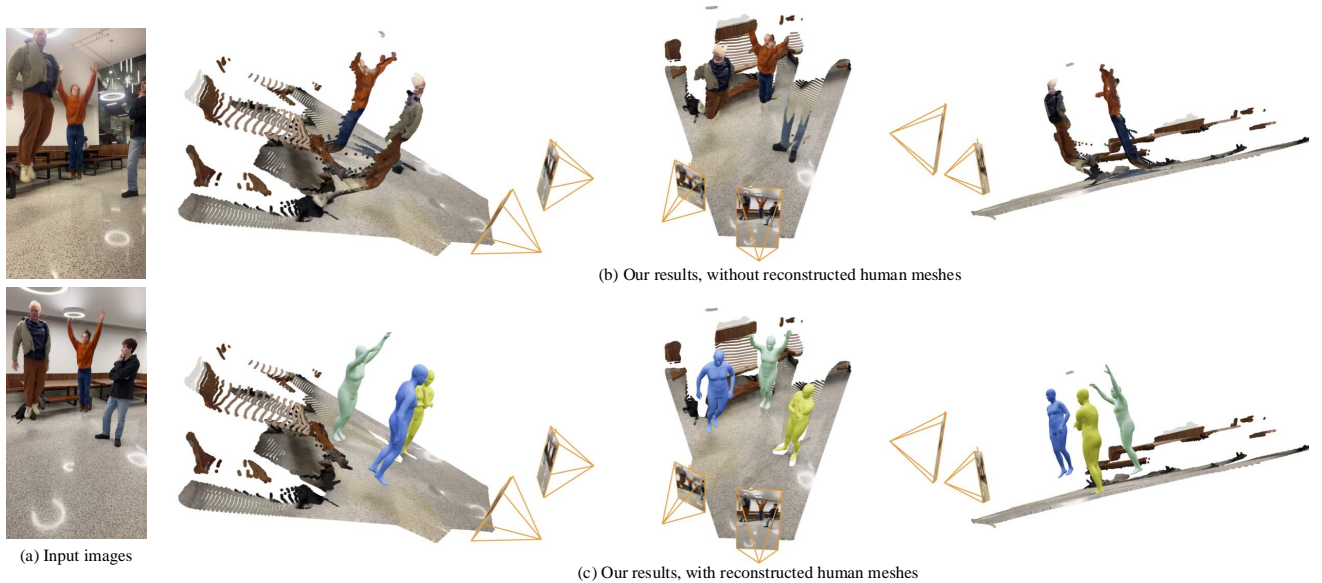


Figure S.1. **Qualitative results in the wild.** We show reconstructions on *in-the-wild* images taken with two smartphones (a), demonstrating the reconstruction of humans and scenes. Unlike previous works [61, 71], which adopt human-scene contact priors that hinder generalization to scenarios without ground foot contact, HSfM recovers accurate world locations of the human meshes that are coherent with the static scene structure. The use of humans in our framework (c) not only serves as a reliable initialization for 3D structure in the SfM formulation but also provides more faithful and complete information about people in the world, which a noisy human point cloud (b) cannot offer. For visualization purposes, the human point cloud is removed using SAM2 [38].

cause the raw camera and scene outputs have a significantly smaller scale than the real world due to their scale normalization during training.

Choosing a large scale value ($\alpha = 100$) generally covers the real-world capture scene sufficiently but does not perform as well as our human-centric scaling approach (W-MPJPE: 1.94m vs. 1.04m). The camera metrics are also worse than ours (e.g., RRA values are 5–7% lower than ours). This implies that, without proper scaling, the opti-

mization is prone to failure due to poor initialization and local minima problems.

One common local minimum observed was humans being placed behind the camera while still reprojecting to the correct pixel locations. To address this, we increased the scale α until all humans were placed in front of all cameras, ensuring positive depth values in all camera coordinate systems. While this initialization produced similar quantitative results in successful cases, it completely failed for 2% of



Figure S.2. **Qualitative results in the wild.** We show reconstructions on *in-the-wild* images taken with two cell phones and the reconstruction of humans and scene. Our method places people in the world and reconstructs accurate human-scene contact, *e.g.* between the person's right foot and box.

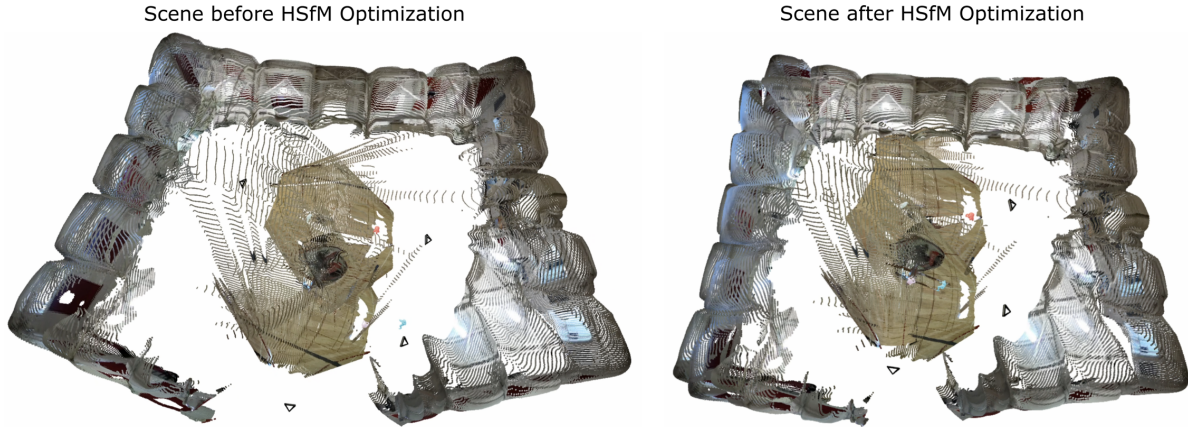


Figure S.3. **Qualitative result of HSfM reconstruction.** Top view of scene from EgoHumans before and after HSfM optimization.

samples, demonstrating that naive initialization approaches are not reliable.

Next, we vary the number of cameras to evaluate the robustness of our method. We tested 2, 4, and 8 input view cameras. As indicated in the table, our joint optimization consistently improves all metrics, regardless of the number of input view cameras. With only 2 cameras, W-MPJPE is 2.63m and GA-MPJPE is 0.26m, indicating accurate human placement in the world. The consistently better camera results compared to the initialization further validate the benefit of incorporating humans into the traditional SfM formulation. The robustness of our method is further demonstrated qualitatively in Figure S.2, where the data is captured by two cameras in in-the-wild scenes.

S.4. Evaluation Details

S.4.1. Evaluation Metrics

In this section, we provide additional details about our human pose and camera metrics.

W-MPJPE describes the mean per-joint position error, measured in the world frame. To bring predicted human meshes into the ground-truth’s world coordinate system, we use an SE(3) rigid alignment from the estimated camera positions to the ground-truth camera positions.

PA-MPJPE describes the Procrustes-aligned variant of MPJPE, which measures position errors after Sim(3) alignment of joints for each human. This metric evaluates local pose accuracy in a way that is not dependent on camera position estimates or human body scale.

GA-MPJPE evaluates group-aligned joint position errors, computed after Sim(3) alignment for all humans in a scene. This measures people relative to each other, without considering the scene or camera positions.

TE measures the mean Euclidean distance between predicted and ground truth camera positions, after SE(3) align-

ment. TE evaluates metric accuracy of camera positions.

s-TE is the scale-aligned version of TE, where we preprocess positions with Sim(3) instead of SE(3) alignment. This measures scale-invariant errors for estimated cameras.

AE measures the average Angle Error between camera pairs. We compute relative orientations for each pair of cameras in a scene. We then measure the difference between ground-truth and predicted pairwise orientations, convert to degrees, and average.

CCA [27] measures the Camera Center Accuracy, after the SE(3) alignment process used for TE. $CCA@τ$ is the proportion of camera positions with absolute error within $τ%$ of the overall scene scale. Following existing work, we compute the scene scale as the furthest distance between a ground-truth camera and the centroid.

s-CCA measures the the scale-aligned version of CCA, after the Sim(3) alignment process used for s-TE.

RRA [52] measures the Relative Rotation Accuracy of camera estimates, computed using the same camera pairs as AE. $RRA@τ$ is the proportion of pairwise camera orientations with angular error of $τ$ degrees or lower.

S.4.2. Evaluation Datasets

EgoHumans: In the main text’s tables and Table S.1’s 4 view case, we used the following camera configurations for each sequence:

- For 01_tagging sequences: camera 1, camera 4, camera 6, and camera 8.
- For 02_lego sequences: camera 2, camera 3, camera 4, and camera 6.
- For 03_fencing sequences: camera 4, camera 5, camera 10, and camera 13.
- For 04_basketball sequences: camera 1, camera 3, camera 4, and camera 8.
- For 05_volleyball sequences: camera 2, camera 4, camera 8, and camera 11.

- For 06_badminton sequences: camera 1, camera 2, camera 5, and camera 7.
- For 07_tennis sequences: camera 4, camera 9, camera 12, and camera 20.

In Table S.1's 2 view case, we used the following camera configurations for each sequence:

- For 01_tagging sequences: camera 1 and camera 2.
- For 02_lego sequences: camera 3 and camera 5.
- For 03_fencing sequences: camera 5 and camera 13.
- For 04_basketball sequences: camera 2 and camera 7.
- For 05_volleyball sequences: camera 6 and camera 12.
- For 06_badminton sequences: camera 5 and camera 7.
- For 07_tennis sequences: camera 9 and camera 12.

In Table S.1's 8 view case, we used the following camera configurations for each sequence:

- For 01_tagging sequences: all 8 available cameras.
- For 02_lego sequences: all 8 available cameras.
- For 03_fencing sequences: camera 1, camera 3, camera 5, camera 7, camera 9, camera 11, camera 13, camera 15.
- For 04_basketball sequences: all 8 available cameras.
- For 05_volleyball sequences: camera 1, camera 3, camera 5, camera 7, camera 9, camera 11, camera 13, camera 15.
- For 06_badminton sequences: camera 1, camera 3, camera 5, camera 7, camera 9, camera 11, camera 13, camera 15.
- For 07_tennis sequences: camera 1, camera 3, camera 5, camera 7, camera 9, camera 11, camera 13, camera 15.

EgoExo4D: EgoExo4D scenes are typically captured using four to six RGB cameras and an egocentric device (Aria glasses). For our experiments and the baselines, we use only the RGB images from sequences with correct re-identification. Sequences containing ego-centric RGB views, such as helmet-mounted cameras, are excluded. We evaluate 182 videos from the validation set, sampling one random frame per video. The videos include ground-truth annotations for human poses, locations, and camera parameters. We evaluate on the following takes/frames:

cmu_soccer06_3/1426
 cmu_soccer12_2/6807
 cmu_soccer16_2/6373
 georgiatech_bike_06_12/170
 georgiatech_bike_06_2/97
 georgiatech_bike_06_6/74

georgiatech_bike_06_8/15
 georgiatech_bike_07_10/28
 georgiatech_bike_07_12/38
 georgiatech_bike_07_2/97
 georgiatech_bike_07_4/46
 georgiatech_bike_07_6/67
 georgiatech_bike_07_8/138
 georgiatech_bike_14_12/593
 georgiatech_bike_14_2/1214
 georgiatech_bike_14_6/575
 georgiatech_bike_14_8/97
 georgiatech_bike_15_2/1508
 georgiatech_bike_15_4/844
 georgiatech_bike_15_6/1103
 georgiatech_bike_15_8/3153
 georgiatech_bike_16_2/882
 georgiatech_bike_16_6/3031
 georgiatech_bike_16_8/1274
 georgiatech_covid_02_10/2227
 georgiatech_covid_02_12/6974
 georgiatech_covid_02_14/2926
 georgiatech_covid_02_2/67
 georgiatech_covid_02_4/67
 georgiatech_covid_04_10/999
 georgiatech_covid_04_12/6160
 georgiatech_covid_04_4/2996
 georgiatech_covid_04_6/4528
 georgiatech_covid_06_2/47
 georgiatech_covid_06_4/64
 georgiatech_covid_18_10/5524
 georgiatech_covid_18_12/3457
 georgiatech_covid_18_2/2413
 georgiatech_covid_18_4/3534
 georgiatech_covid_18_6/4389
 georgiatech_covid_18_8/458
 iiith_cooking_59_2/7795
 iiith_cooking_64_2/298
 iiith_cooking_89_6/1177
 iiith_cooking_90_4/1383
 iiith_soccer_015_2/1610
 nus_cpr_12_1/1338
 nus_cpr_12_2/76
 sfu_basketball012_10/774
 sfu_basketball012_12/399
 sfu_basketball012_2/945
 sfu_basketball012_3/1506
 sfu_basketball012_4/66
 sfu_basketball012_6/526
 sfu_basketball012_7/1581
 sfu_basketball012_8/329
 sfu_basketball016_2/247
 sfu_basketball_04_8/209
 sfu_basketball_05_22/1902

sfu_basketball_05_26_29
sfu_basketball_09_11_32
sfu_basketball_09_12_1114
sfu_cooking028_12_1049
sfu_cooking_007_7_77
sfu_cooking_008_3_4164
sfu_cooking_008_5_3559
sfu_covid_004_2_2828
sfu_covid_004_4_5360
sfu_covid_008_16_1595
unc_basketball_02-24-23_01_3_84
unc_basketball_02-24-23_02_10_466
unc_basketball_02-24-23_02_11_927
unc_basketball_03-30-23_02_10_45
unc_basketball_03-30-23_02_14_7
unc_basketball_03-30-23_02_15_40
unc_basketball_03-30-23_02_17_9
unc_basketball_03-30-23_02_18_20
unc_basketball_03-30-23_02_19_7
unc_basketball_03-30-23_02_4_107
unc_basketball_03-30-23_02_5_25
unc_basketball_03-30-23_02_7_1141
uniandes_basketball_001_23_768
uniandes_basketball_001_24_1386
uniandes_basketball_001_26_146
uniandes_basketball_001_27_439
uniandes_basketball_003_38_32
uniandes_basketball_004_23_369
uniandes_basketball_004_44_261
uniandes_basketball_004_45_667
uniandes_dance_002_11_201
uniandes_dance_002_2_439
uniandes_dance_008_29_276
uniandes_dance_008_30_166
uniandes_dance_008_31_31
uniandes_dance_008_32_11
uniandes_dance_008_33_1105
uniandes_dance_008_34_753
uniandes_dance_008_35_607
uniandes_dance_008_36_1045
uniandes_dance_008_37_913
uniandes_dance_008_38_706
uniandes_dance_016_10_841
uniandes_dance_016_11_279
uniandes_dance_016_12_932
uniandes_dance_016_13_453
uniandes_dance_016_14_951
uniandes_dance_016_30_577
uniandes_dance_016_31_1709
uniandes_dance_016_32_377
uniandes_dance_016_33_1158
uniandes_dance_016_36_1247
uniandes_dance_016_37_145
uniandes_dance_016_38_1416
uniandes_dance_016_39_399
uniandes_dance_016_3_1239
uniandes_dance_016_42_1406
uniandes_dance_016_43_1271
uniandes_dance_016_44_1268
uniandes_dance_016_45_838
uniandes_dance_016_6_1361
uniandes_dance_016_7_1040
uniandes_dance_016_8_1488
uniandes_dance_017_6_1592
uniandes_dance_019_17_1003
uniandes_dance_019_18_509
uniandes_dance_019_19_1537
uniandes_dance_019_20_1089
uniandes_dance_019_22_81
uniandes_dance_019_24_484
uniandes_dance_019_25_183
uniandes_dance_019_26_1814
uniandes_dance_019_27_283
uniandes_dance_019_28_1411
uniandes_dance_019_46_412
uniandes_dance_019_47_790
uniandes_dance_019_49_1617
uniandes_dance_019_51_481
uniandes_dance_019_52_875
uniandes_dance_019_54_766
uniandes_dance_019_55_679
uniandes_dance_019_56_561
uniandes_dance_019_57_1073
uniandes_dance_019_58_192
uniandes_dance_024_11_1619
uniandes_dance_024_12_104
uniandes_dance_024_13_1419
uniandes_dance_024_14_1180
uniandes_dance_024_15_378
uniandes_dance_024_16_1569
uniandes_dance_024_17_1317
uniandes_dance_024_45_844
uniandes_dance_024_47_732
uniandes_dance_024_48_261
uniandes_dance_024_49_325
upenn_0706_Dance_4_2_2512
upenn_0706_Dance_4_3_1277
upenn_0706_Dance_4_4_1670
upenn_0706_Dance_4_5_1904
upenn_0713_Dance_3_2_164
upenn_0713_Dance_3_3_586
upenn_0713_Dance_3_4_0
upenn_0713_Dance_3_5_243
upenn_0713_Dance_4_2_125
upenn_0713_Dance_4_3_1280
upenn_0713_Dance_4_4_308

upenn_0713_Dance_4_5/262
upenn_0713_Dance_5_4/238
upenn_0713_Dance_5_6/2534
upenn_0721_Piano_1_2/140
upenn_0721_Piano_1_3/648
upenn_0722_Piano_1_2/83
upenn_0727_Partner_Dance_3_1_2/62
utokyo_pcr_2001_29_2/5799
utokyo_pcr_2001_29_4/3491
utokyo_pcr_2001_29_6/550
utokyo_pcr_2001_30_2/2121
utokyo_pcr_2001_30_4/1696
utokyo_pcr_2001_32_2/6641
utokyo_pcr_2001_32_4/6048
utokyo_soccer_8000_43_2/3262
utokyo_soccer_8000_43_4/3472
utokyo_soccer_8000_43_6/2781

S.5. Implementation Details

Given sparse-view images, HSfM jointly estimates SMPL-X [35] parameters for humans, scene pointmaps, and camera poses (rotation and translation), in the world coordinate frame. The SMPL-X parameters for humans are initialized using predictions from HMR2 [16] converted to SMPL-X following the conversion procedure in [33]. Scene pointmaps and camera parameters are initialized with estimates from DUSf3R [53]. We use Adam [25] optimizer and set the number of optimization steps proportional to the scene scale with a minimum of 500 steps. This allows sufficient time to accurately determine scene scale and camera poses and people’s location. The learning rate is set to 0.015 with a linear reduction schedule. To tune hyperparameters, we use the first frame (4 cameras) of sequences 01_tagging and 04_basketball of EgoHumans as these scene encompass a good range of scene scales.

S.6. Additional related work

Monocular Human Mesh Reconstruction. Most methods estimate 3D humans in the camera coordinate system for a single person [14, 16, 23, 35] or for multiple people with depth estimation [2, 46, 67]. Recent works jointly estimate human and camera motion in the world coordinate frame [29, 43, 44, 47, 54, 61, 65, 69]. They leverage temporal dynamics from video sequences to improve reconstruction quality over time. While single-view reconstruction methods are valuable for their minimal input requirements, they often suffer from ambiguity, especially due to occlusion. Our approach leverages multi-view data to enhance reconstruction accuracy and integrates scene context, providing a more detailed and reliable reconstruction of multi-person interactions within their environment.

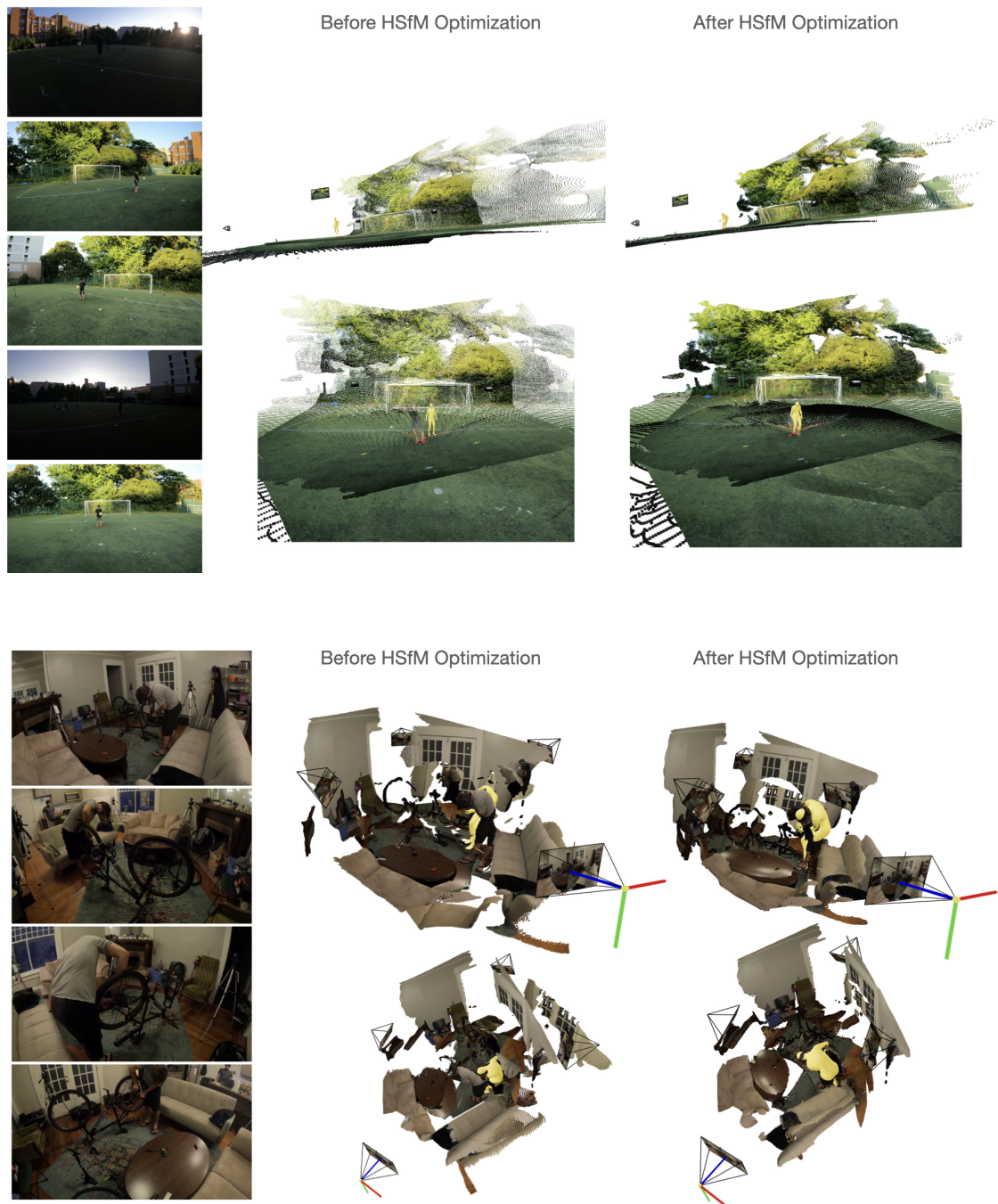


Figure S.4. **Qualitative results.** We show reconstruction on EgoExo4D. On the left, the input images to our method, the scene, humans, and cameras before optimization (HSfM (init.)) in the center, and the reconstruction of our method after joint optimization on the right.

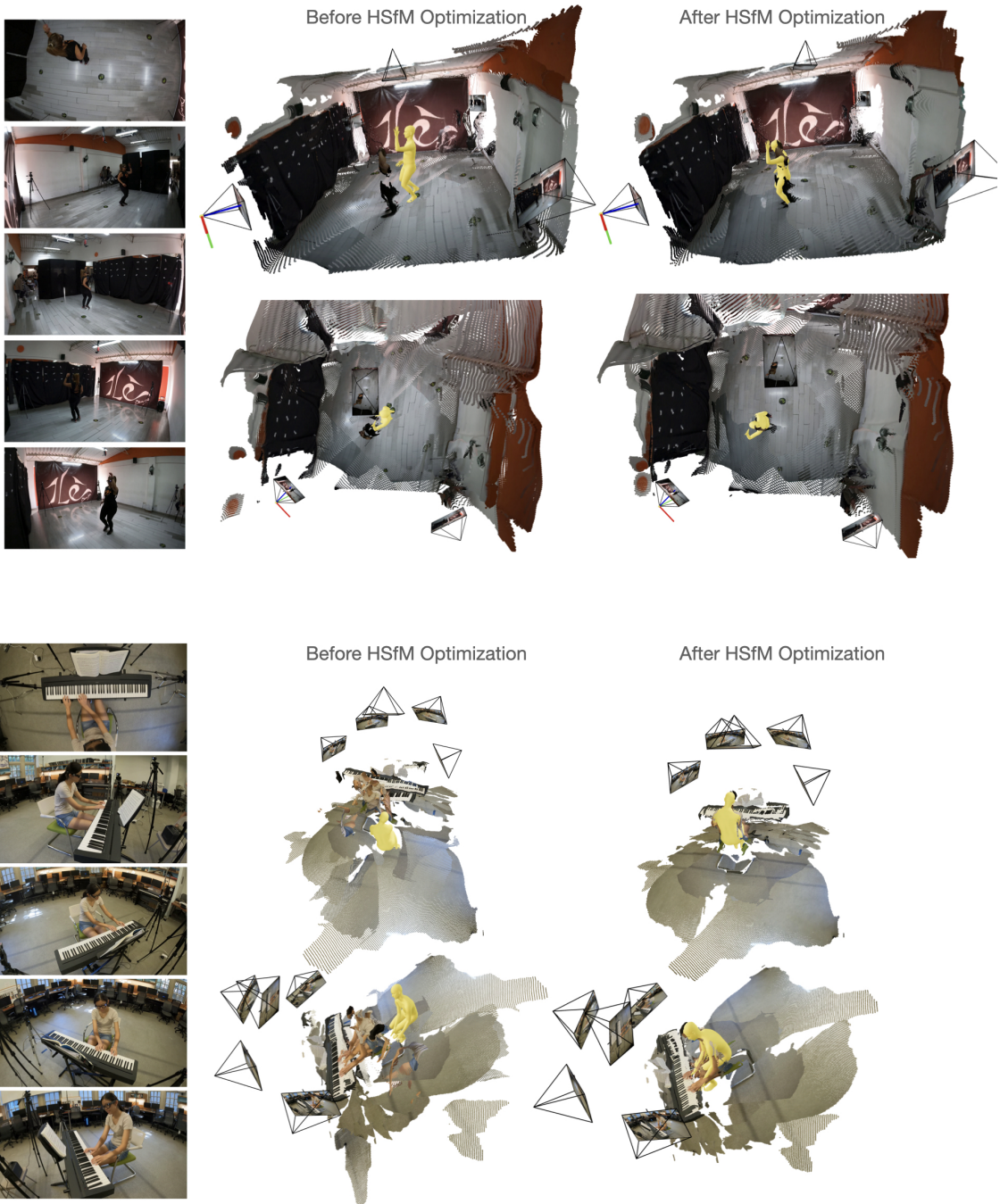


Figure S.5. Continuation of Fig. S.4



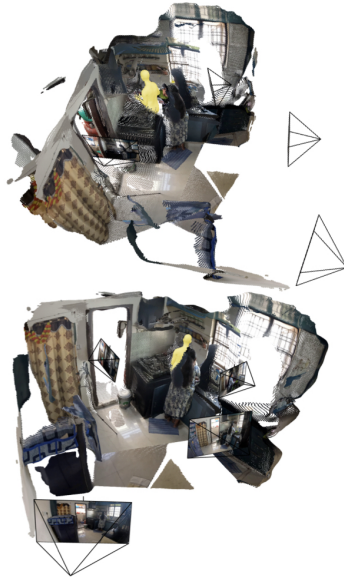
Before HSfM Optimization



After HSfM Optimization



Before HSfM Optimization



After HSfM Optimization

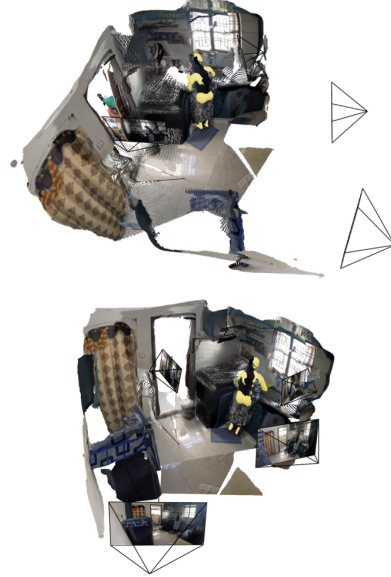


Figure S.6. Continuation of Fig. S.4

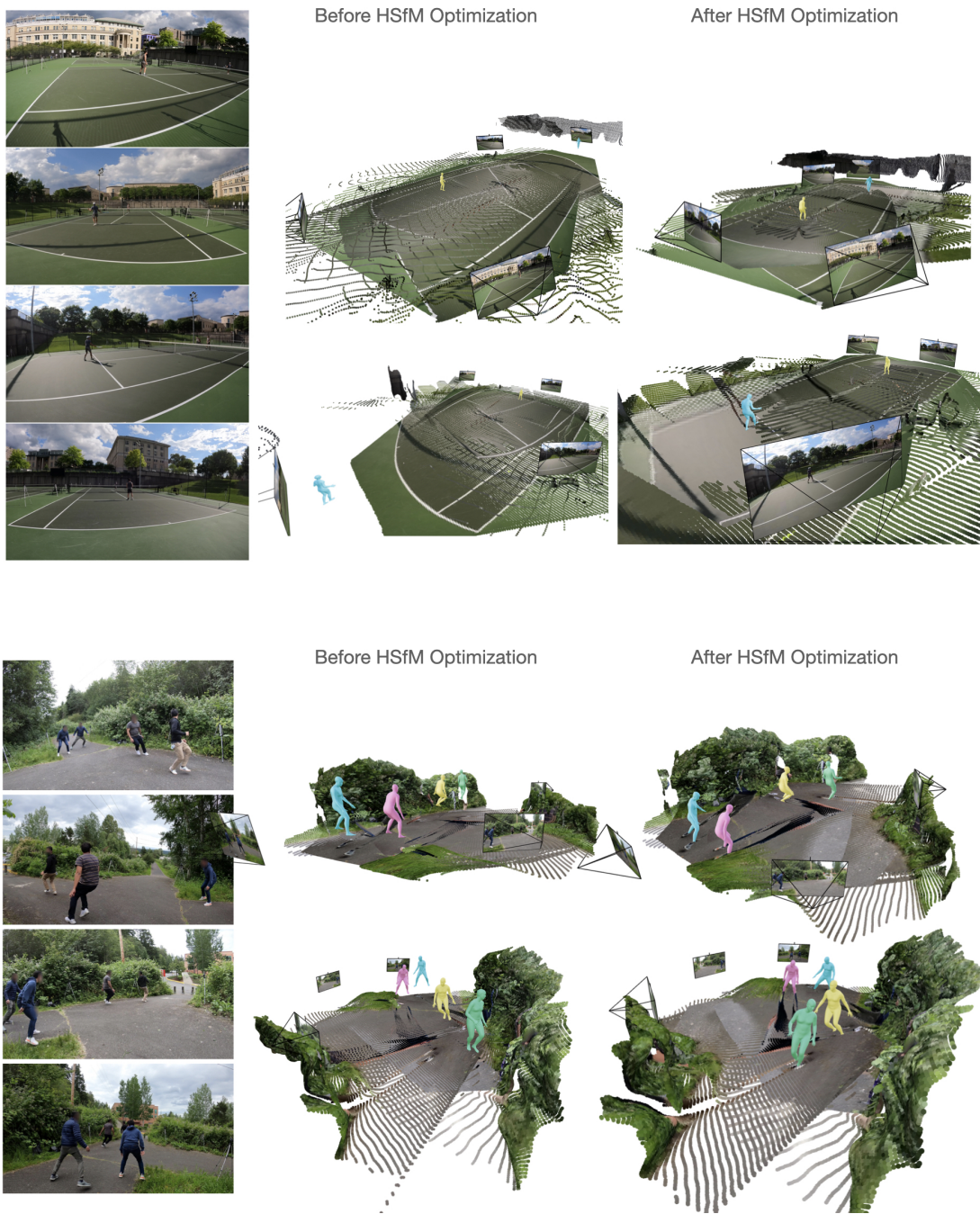
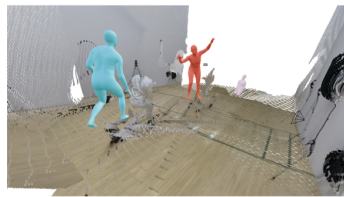


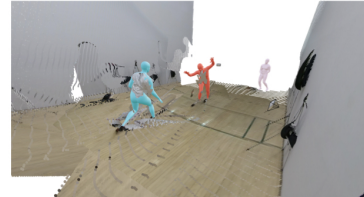
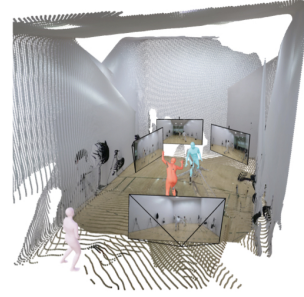
Figure S.7. **Qualitative results.** We show reconstructions on EgoHumans. On the left, the input images to our method, the scene, humans, and cameras before optimization (HSfM (init.)) in the center, and the reconstruction of our method after joint optimization on the right.



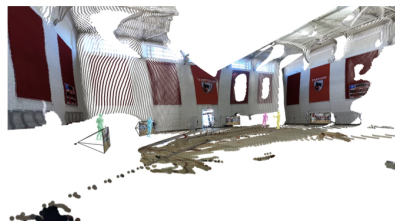
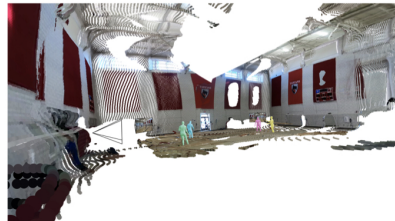
Before HSfM Optimization



After HSfM Optimization



Before HSfM Optimization



After HSfM Optimization

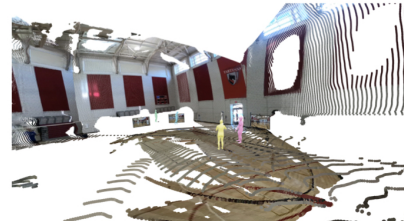


Figure S.8. Continuation of Fig. S.7